Turk J Phys
33 (2009) , 87 – 100.

doi:10.3906/fiz-0803-7

Electrical Characterization and Relaxation Behavior of Lithium-Indium-Phosphate Glasses via Impedance Spectroscopy

M. V. N. V. D. SHARMA[1], A. V. SARMA[1], R. Balaji RAO[2]
[1]*Andhra University, Department of Physics Visakhapatnam, 530 003 Andhra Pradesh-INDIA*
e-mail: sarmavakella@yahoo.co.in
[2]*Department of Physics, GITAM, Institute of Technology, GITAM University, Visakhapatnam, 530045, Andhra Pradesh-INDIA*
e-mail: ravuri3091@yahoo.co.in

Received 12.03.2008

Abstract

Phosphate glasses with various compositions of lithium oxide and indium oxide were synthesized by melt quenching technique. The glass forming ability parameter K_{gl} was characterized by differential thermal analysis. The electrical measurements for all the glass samples were carried out in the frequency range of 10 Hz to 10^6 Hz and at a temperature range of 393–513 K by the Impedance spectroscopy. Frequency dependent conductivity follows the power law. The ac conductivity increases with temperature following the Arrhenius law. Master curve in the scaling analysis suggesting the temperature independent conduction relaxation mechanism.

Key Words: Phosphate glass structure, Differential thermal analysis, Electrical properties.

1. Introduction

Among the lithium based glass electrolytes, lithium phosphates are established glass forming systems owing to their technological significance in various applications such as lithium ion batteries, gas sensors, electro chromic displays, etc. [1–4]. Lithium phosphate glasses are found to exhibit high ionic conductivity than other crystals, since these glasses possess more open structure for ionic transport. These glasses can be prepared in varied compositions with high structural flexibility, homogeneity, chemical durability and posses excellent physical properties like high thermal expansion coefficients, low melting and softening temperatures, high ultra violet (UV) and far-infrared (IR) transmission [5–7]. The basic phosphate glass network structure consists

of interconnected PO_4 tetrahedra. Addition of Li_2O into the phosphate glass system introduces coordinated defects along with non-bridging oxygen ions, and also acts as network modifier and breaks P–O–P linkages. Generally, Li^+ ions sit in the vicinity of these non-bridging oxygen sites and ionic conductivity is believed to arise from non-random hopping of Li^+ ion between these sites under the influence of an external field. It is well recognized that the variation in the conductivity is due to the structural change of the glass with composition; consequently it is attractive to be aware of the movement of mobile ions in the glasses by interpreting the frequency and temperature dependent features in their dielectric response.

Addition of IIIA group oxides like Al_2O_3, Ga_2O_3 and In_2O_3 have been observed to be good stabilizers of phosphate glasses and these oxides are expected to improve the physical properties to a considerable extent and thereby enhance the range of applicability of these glasses [8–10]. Among them, Indium oxide (In_2O_3) is a n-type semiconductor, useful in glass coloring, in alkaline batteries to suppress gassing, as an anti-arcing additive in high current electrical switches and contactors. In addition, it is used as resistive element in integrated circuits and to form hetero junctions with p-InP, n-GaAS and other semiconductors. The presence of In_2O_3 in the lithium phosphate glasses is projected to enhance chemical solubility, improves the aqueous corrosion, transparency and act as both network modifier and network former in the glass network [11, 12]. The additional probable influence of indium oxide in the Li_2O-P_2O_5 glass network is that there is every possibility for the formation of local nanocrystals of In_2O_3 which possess large polarizabilities. This is justified because the indium oxide is able to form very low dimensional nanoparticles which have substantial polarizabilities influencing the surrounding structural clusters [13]. Detailed structural studies of the present investigation of these glasses were studied using DSC, and the electrical properties as a function of frequency and temperature were studied through impedance spectroscopy in view of the fact that this technique is a power full tool to probe in the glass materials [14–17].

2. Experimental

Glass samples of compositions selected for the present investigation are given in Table 1. Appropriate proportions of annular grade reagents of Li_2CO_3, In_2O_3 and P_2O_5 were thoroughly mixed in an agate mortar and melted in a platinum crucible at 800 ± 10 °C for about 1 h until a bubble-free liquid was formed. The resultant melt was then cast in a brass mould and subsequently annealed at 300 °C. The amorphous state of the glasses was checked by the X-ray diffraction method. The Differential thermal analysis were recorded simultaneously at heating rate of 20 K/min in the temperature range of 300–673 K using a-Al_2O_3 as a reference material by using a DT-30 Schimadzu thermal analyzer. The DTA thermograms of all samples showed the glass transition temperature T_g. The accuracy in the measurement of T_g is ± 2 K. The samples were then ground and optically polished. The final dimensions of the samples used for the electrical measurements were about 1 cm × 1cm × 0.2 cm. A thin coating of silver paint was applied (to the larger area faces) on either side of the glasses to serve as electrodes for electrical measurements. The real (Z') and imaginary (Z'') parts of the impedance of present glasses were obtained using a Solatron 1260 Impedance/Gain Phase analyzer controlled by personal computer in the frequency range of 10 Hz–10^6 Hz at room temperature and as well as temperatures from 303–523 K with a 10 K temperature step.

Table 1. Details of the compositions of the glasses.

Glass	Li_2O (mol%)	In_2O_3 (mol%)	P_2O_5 (mol%)
L_{20}	20	20	60
L_{22}	22	18	60
L_{24}	24	16	60
L_{26}	26	14	60
L_{28}	28	12	60
L_{30}	30	10	60
L_{32}	32	08	60

3. Results and Discussion

3.1. Differential thermal analysis

The DTA thermograms of Li_2O-In_2O_3-P_2O_5 glass system with various compositions are shown in Figure 1. The appearance of single peak due to the glass transition temperature in DTA pattern of all the glasses indicates the homogeneity of the glasses prepared. The thermograms of all the glass samples exhibit an endothermic effect due to glass transition temperature T_g. The value of T_g is evaluated from the point of inflection of this change. At higher temperatures, an exothermic peak T_c due to the crystal growth followed by another endothermic effect due to the re-melting of the glass is also observed. The glass transition temperature T_g values are gradually decreases with increases in the concentration of Li^+ ions (from the glass sample L_{20} (20 mol% Li_2O) to L_{28} (28 mol% Li_2O). This can be ascribed due to increasing de-polymerization of the glass network, due to increase in the modifier Li^+ ions concentration to form a large number of non bridging oxygen sites. Increasing T_g from L_{28} (28 mol% Li_2O) to L_{32} (32 mol% Li_2O), there is decrease in the de-polymerization of the glass network [8, 9], due to the effect of indium ions that take part in the network forming positions with the glass former. Variation of the glass forming ability parameter $K_{gl} = (T_c - T_g)$ / $(T_m$ - $T_c)$ with the concentration of Li_2O is plotted in Figure 2. The lowest value of K_{gl} for glass sample L_{28} indicates the highest degree of disorder, as the indium ions may prefer to occupy network modifying positions within the favored concentrations.

3.2. Electrical characterization

The electrical characterization of Li_2O-In_2O_3-P_2O_5 glass system with various compositions was monitored using impedance spectroscopy. This technique utilizes alternating current with variable frequency and when measurements are carried out as a function of frequency and temperature, it is possible to determine the activation energies of the conduction and dielectric relaxation processes [15–17]. The complex impedance (Z'' vs. Z') plots of all the glass samples measured at 393 K and for the highest conducting sample L_{28} at different temperatures (393–503 K) were found to exhibit complete semicircles, as depicted in Figure 3 and Figure 4. The bulk resistance R for all the samples relative to each experimental temperature is deduced from the intercept of imaginary impedance (Z'') with real (Z′) impedance axes. The impedance data obtained in this work was fitted to nonlinear least-square method. Hence the electrical response can be associated to a parallel resistance–capacitance (RC), equivalent circuit and therefore bulk response of the glass is detected.

The resistance R obtained from the analyzed impedance data and pellet dimensions were used to calculate the bulk conductivity of all the glass samples at 393 K and for the glass sample L_{28} at different temperatures.

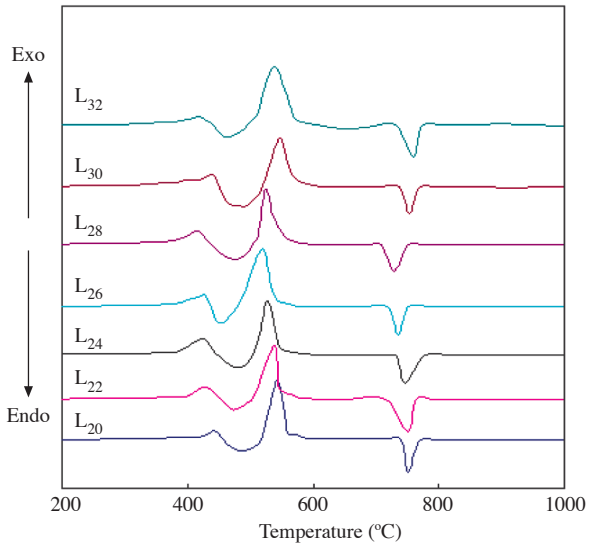

Figure 1. Differential thermal analysis traces of for all the samples of Li_2O-In_2O_3-P_2O_5 glass system.

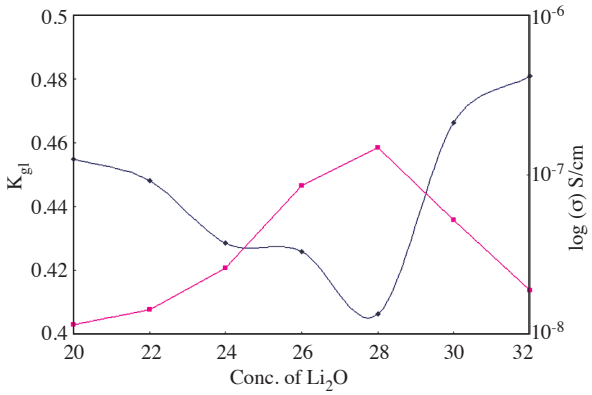

Figure 2. Variation of glass forming ability parameter (K_{gl}) and log(σ) (at 393 K) with the concentration of Li_2O for all the glass samples with various compositions of Li_2O-In_2O_3-P_2O_5 glass system.

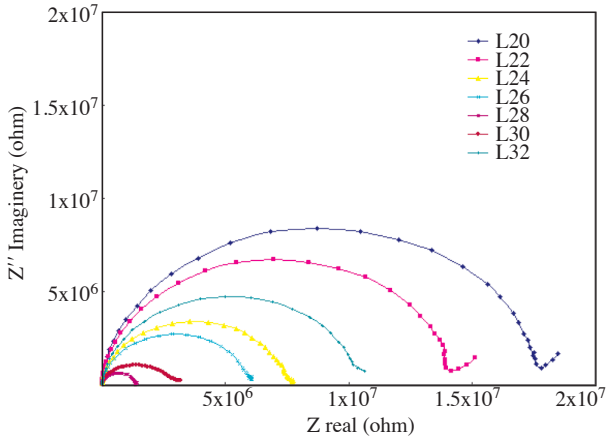

Figure 3. Complex impedance spectra (Z'' versus Z') for all the samples of Li_2O-In_2O_3-P_2O_5 glass system measured at 393 K.

The bulk conductivity can be calculated by taking sample geometry into account as follows:

$$\sigma = (1/R) \times (t/A), \tag{1}$$

where t is the sample thickness, A is the electrode area used to measure the properties of the sample and t/A is the sample geometric ratio.

Using above equation, one can deduce that the highest conductivity is achieved by the L_{28} sample (σ 1.477×10^{-7} S/cm, at 393 K). In Figure 4, we show the characteristic complex impedance plots at different temperatures for the highest conducting sample L_{28}, where it can be seen that increases in temperature caused the impedance semicircles to be shifted to lower and lower Z' values. Once again, one can use the intersection points of the imaginary impedance onto the real axis of semicircles to use equation (2) to calculate the bulk conductivity of all the glass samples as a function of temperature. The bulk conductivities calculated from the analyzed impedance data obtained at different temperatures for all the glass samples are plotted in Figure 5 (shown as log σT versus $1000/T$).

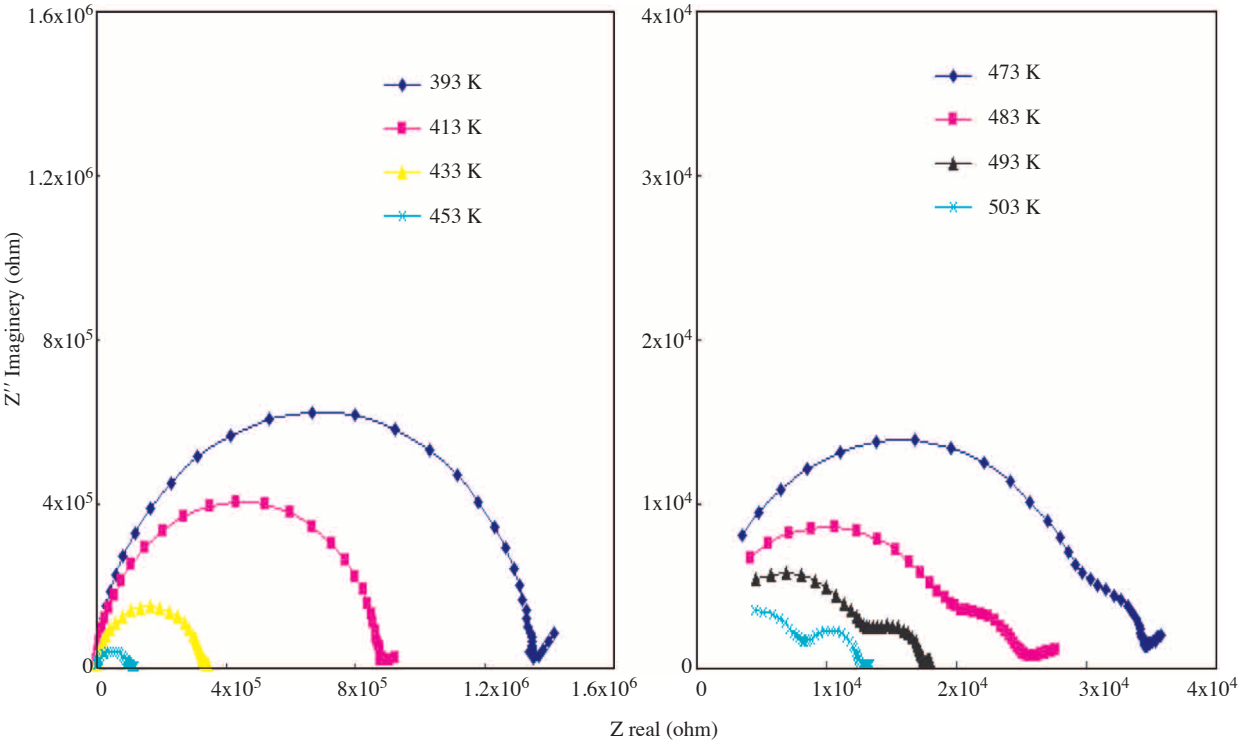

Figure 4. Complex Impedance spectra (Z'' versus Z') for the highest conducting sample, L_{28}, at temperatures 393–503 K.

The conductivity data is fitted to the Arrhenius equation

$$\sigma = \sigma \exp(-E_{a\sigma}/k_B T), \tag{2}$$

where σ_0 is the pre exponential factor and $E_{a\sigma}$, k_B and T are the activation energy for the conduction, Boltzman's constant and absolute temperature respectively. The activation energy for conduction ($E_{a\sigma}$) was calculated from the slope of the straight lines obtained when the data is plotted against $1000/T$ of all the glass samples with various compositions (Figure 5). The composition dependence of activation energy ($E_{a\sigma}$) at 393 K is shown in the inset of Figure 5. It is observed that the activation energy is found to be the minimum for highest conducting glass sample (L_{28}). Since the inset of Figure 5 (activation energy $E_{a\sigma}$, versus concentration of lithium oxide) does not show the non linear behavior of conductivity; the non linearity between

the conductivity and the activation energy suggests that the conductivity enhancement is directly related to the increasing mobility of the charge carriers [18]. The indium ions can be considered as immobile within the time window of hopping processes of the alkali (Li^+) ions, the contribution to the conduction for the samples investigated in this paper can be renowned mainly due to motion of Li^+ ions [19]. This is further affected by the presence of the indium ions as will be described next. It is speculated that Raman spectra for glass samples revealed the presence of Li_2O in the glass network results in the formation of large number of non bridging sites, where the Li^+ ions are weakly bonded to non bridging sites. As it appears, due to the increasing modifying action of the Li^+ ions, for compositions up to 28 mol% of Li_2O, easy paths for the movement of the charge carriers are created and hence increase in the conductivity is observed. However, when Li_2O concentration is increased from 28 mol% to 32 mol% in the glass matrix, the conductivity is observed to decreases gradually with corresponding increase in activation energy as a result of large repulsion between the same Li^+ ions and due to blocking of network forming indium ions by rigidly bound Li^+ ions. Hence, the variation of conductivity with concentration of lithium and indium ions depends heavily on the structural modifications of the glass system [20].

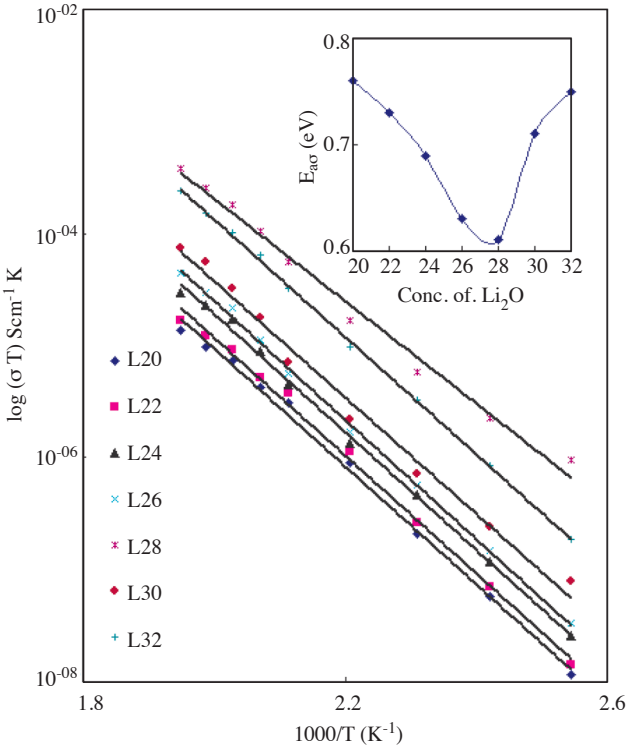

Figure 5. Variation of conductivity $\log(\sigma T)$ as a function of $1000/T$ for all the samples of Li_2O-In_2O_3-P_2O_5 glass system. Inset gives the variation of activation energy $E_{a\sigma}$ with concentration of lithium oxide.

In order to evaluate conductivity non-linearities, it is useful to present the ac conductivity for all the compositions of Li_2O-In_2O_3-P_2O_5 glass system. The dependence of the electrical conductivity with the frequency can be analyzed by the power law equation

$$\sigma_{(ac)} = \sigma(0) + A\omega^s, \tag{3}$$

where $\sigma(0)$ is the conductivity at zero frequency, which is normally termed the dc conductivity; A is a constant; and s is a characteristic parameter ($0 < s < 1$). The low frequency part of the conductivity is normally frequency independent and the frequency independent conductivity ($\sigma(0)$) is obtained by extrapolation of the conductivity to $\omega = 0$. The high frequency part of the conductivity exhibits the dispersion and increases in a power-law fashion [21]. Typical plots of ac conductivity as a function of frequency at 393 K for all glass samples are presented in Figure 6. Similarly, the ac conductivities for the highest conducting glass sample L_{28} at different temperatures are shown in Figure 7. The values of $\sigma(0)$ or σ_{dc} obtained for all the samples at 393 K (from Figure 2) are listed in Table 2. From Figure 7, it can be seen that the critical frequency ($\omega_p = f_o$), at which the conductivity deviates from the frequency independent part changes with the Li_2O concentration. The change in the critical frequency is a more obvious for the ac conductivity of L_{28} at different temperatures presented in Figure 7. Nevertheless, the relation between frequency independent conductivity $\sigma(0)$ and the critical frequency (f_o) can be epresented by the equation

$$\sigma(0) = Kf_o, \tag{4}$$

where $K = (Ne^2a^2/k_BT)\nu c(1\text{-}c)$, is the empirical constant; ν is the geometrical factor which includes a correlated factor; c is the concentration of mobile ions on N equivalent lattices per unit volume; a is the hopping distance; e is the electronic charge; T is absolute temperature; and k_B is Boltzman's constant, which depends on the concentration of mobile ions, temperature and the conduction mechanism [22, 23].

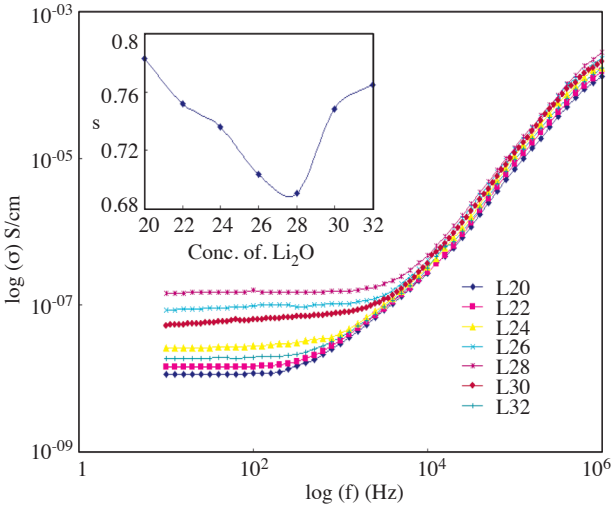

Figure 6. Plots of $\log(\sigma)$ as a function of $\log(f)$ for all samples of Li_2O-In_2O_3-P_2O_5 glass system measured at 393 K. Inset shows the variation of characteristic parameter s with concentration of Li_2O.

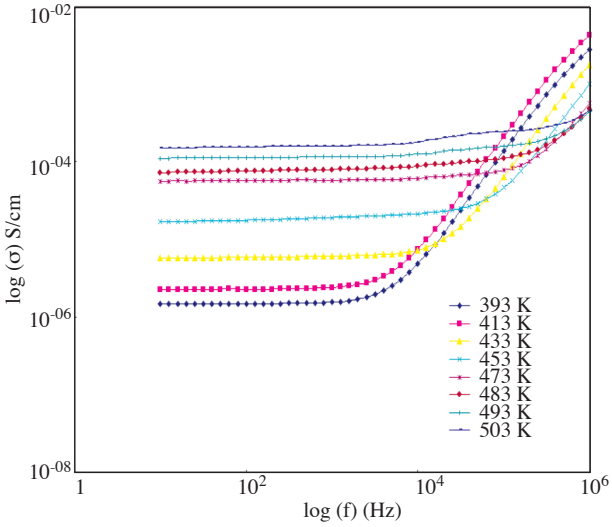

Figure 7. Plots of $\log(\sigma)$ as a function of $\log(f)$ for highest conducting sample, L_{28}, at temperatures 393–503 K.

It has been observed that the relaxation effects begin to appear at the critical frequency f_o and moves towards the higher frequency with in the wider experimental frequency range. Further, it is observed that the critical frequency f_o is thermally activated with same activation energy as $\sigma_0 T$ [24]. The characteristic parameter s has been observed to be material dependent and calculated from equation (4). The variation of

characteristic parameter s with the concentration of Li_2O is shown in the inset of Figure 6 and it is observed that s is found to be lowest for the highest conducting glass sample, L_{28}. The minimum value of s is found to be related to the high degree of modification and is found to be dependent on the concentrations of Li^+ ions and network modifying indium ions; however, the increasing value of s from L_{28} to L_{32} is due to the presence of the indium ions that are present predominantly in network forming sites at lower concentrations. The frequency independent part of the conductivity may be attributed due to the long-range transport of Li^+ ions and the frequency dependent part of the conductivity could be explained through the diffusion controlled relaxation model [25]. The summary of electrical conductivity, activation energy, and characteristic parameter is listed in the Table 2.

Table 2. Summary of Conductivity, activation energy, characteristic parameter and critical frequency for all compositions of Li_2O-In_2O_3-P_2O_5 glass system.

Glass	σ (393 K) S/cm	$E_{a\sigma}$ (eV)	s (393K)	$E_{a\tau}$ (eV)	β (393 K)	$\tau(10^{-4}$ sec) at 393 K
L_{20}	1.14E-08	0.76	0.783	0.76	0.684	0.425
L_{22}	1.43E-08	0.73	0.752	0.72	0.674	0.555
L_{24}	2.59E-08	0.69	0.736	0.68	0.668	1.329
L_{26}	8.51E-08	0.63	0.704	0.61	0.653	1.751
L_{28}	1.48E-07	0.61	0.691	0.60	0.647	2.079
L_{30}	5.18E-08	0.71	0.748	0.71	0.662	1.158
L_{32}	1.87E-08	0.74	0.765	0.75	0.68	0.605

3.3. Relaxation behavior

The relative real (ε') and imaginary (ε'') arts of the dielectric constant and the electric modulus were evaluated in the frequency range 10 Hz to 10^6 Hz, for all compositions of Li_2O-In_2O_3-P_2O_5 glass system. Figure 8a and Figure 8b show frequency dependence of real (ε') and imaginary (ε'' arts of dielectric constant for the highest conducting glass sample L_{28} at different temperatures. It is observed that the real (ε') and imaginary (ε'' arts of dielectric constant decrease with increasing frequency at all temperatures evaluated and the values of (ε') and ε'' are observed to exhibit considerable frequency dispersion in the lower frequency range. It is speculated that the increasing dielectric constant (ε') in the lower frequency region is due to contribution of charge accumulation at the interface. However, in the higher frequency region, the contribution of charge accumulation is minimal and hence ε' remains relatively constant. The inset of Figure 8a shows variation of dielectric constant (ε') with concentration of lithium oxide, taken from the highest frequency region (100 kHz) where it is nearly frequency independent. It has been observed that the highest conducting glass sample L_{28} possesses the highest dielectric constant (ε'). The imaginary part ε'' is dominated by the dc conductivity and will not be discussed further. The dielectric constant response of a material is due to electronic, ionic, dipolar and space charge polarizations. Out of these, the space charge contribution depends upon the purity and the perfection of the glasses. Its influence is in general negligible at very low temperatures and noticeable only in the low frequency region. The dielectric constant behavior as a function of frequency is related to the application of electric field, which supports the electron jumping between filled and empty states in the glass network. Recollecting the data, the increasing trend in the dielectric constant ε' particularly at low frequency region for

the present glass samples may be ascribed to the defects produced in the glass network, which contributes to the electrode polarization [26].

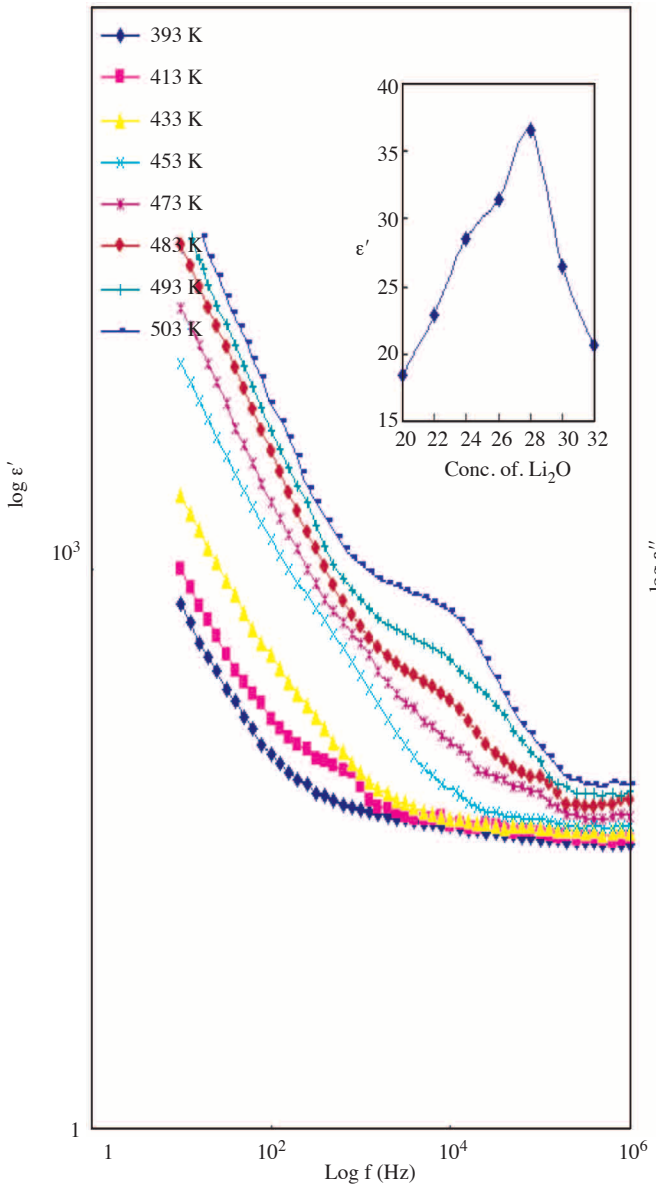

Figure 8a. Variation of real part of dielectric constant ε' with the frequency for the highest conducting sample (L_{28}) at temperatures 393–503 K. Inset shows the variation of ε' with the concentration of Li_2O.

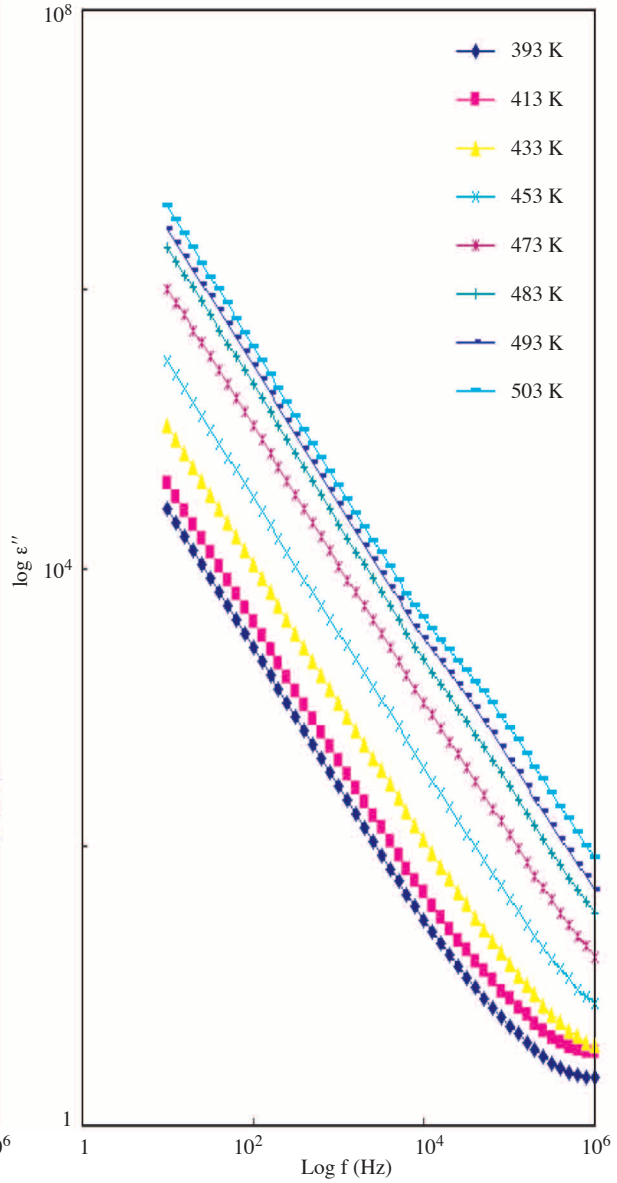

Figure 8b. Variation of Imaginary part of dielectric constant, ε'' with the frequency for the highest conducting sample, L_{28}, at temperatures 393–503 K.

Another approach to probe the electrical response of materials containing some degree of ionic conductivity is to use the complex electric modulus $M^*(\omega) = M' + \mathrm{j}M''$, where M' is the real part of the electric modulus, M'' is the imaginary part of electric modulus. This formulation is predominantly appropriate to identify phenomena as electrode polarization and bulk phenomenon such as average conductivity relaxation

times τ_σ [7, 28].

The complex electrical modulus M^* is related to the complex impedance as described in the equation below:

$$M*(\omega) = j\omega C_o Z*(\omega), \tag{5}$$

where C_o is the geometric capacitance of the cell, ω is the angular frequency and $j = \sqrt{-1}$. The dependence of electric modulus on frequency is given by

$$M*(\omega) = \frac{1}{\varepsilon_s}\left[1 - \int_0^\infty dt \exp(-j\omega t)\left(-\frac{d\varphi}{dt}\right)\right], \tag{6}$$

where ε_s is the dielectric constant at high frequency limit and $\phi(t)$ is the relaxation function.

Variation in the imaginary part of electric modulus M'' with the frequency obtained for all the compositions of Li_2O-In_2O_3-P_2O_5 glass samples at 393 K is shown in Figure 9. Values of M'' show typically asymmetric peaks, and this peak begins from the nature of relaxation behavior. The relaxation behavior and the skew nature of the M'' curves with the variation of lithium oxide concentration obviously suggests the impenetrability of inter-ionic interactions due to the existence of a large number of non-bridging sites in the vicinity. The M'' for the present glasses under investigation is reasonably fitted to Kohlrausch-Williams-Watts function for relaxation (KWW) [29]:

$$\phi = \phi_0 \exp\left[-\left(\frac{t}{\tau}\right)^\beta\right], \tag{7}$$

where τ is the characteristic relaxation and β is the stretched exponent and its value lies in between 0 and 1. Full width at half maximum (β) of M'' peaks are shown in the inset of Figure 9. β is the smallest for the highest conducting sample L_{28}, obviously suggesting the presence of both the mobile lithium ions and network modifying indium ions in the neighborhood of conduction path. Figure 10 shows the imaginary part of electric modulus M'' dependence with the frequency of highest conducting glass sample L_{28} at different temperatures. It can be observed that the M'' value is observed to be constant ($M''_{\max}$) at a relaxation frequency $f_{\max}$ and the peak $M''_{\max}$ symmetrically shifts towards higher frequencies with increasing temperatures. From Figure 10, the relaxation frequency $f_{\max}$ corresponding to maximum in M'' curves and the relaxation time τ as calculated using the relation $\tau = 1/2\pi f_{\max}$ at different temperatures can be obtained. The experimental data are well described by the Arrhenius expression, given as below:

$$\tau = \tau_0 \exp(E_{a\tau}/T\kappa) \tag{8}$$

where τ_0 is the pre-exponential factor and $E_{a\tau}$ is the activation energy for conductivity relaxation.

The variation of $\log \tau$ with $1000/T$ for all the compositions of glass at different temperatures is shown in Figure 11. It can be observed that the relaxation time τ symmetrically shifts to higher values with an increase in temperature. The activation energy for the conductivity relaxation $E_{a\tau}$ of all the glass samples was calculated from the relaxation time plots. The similarity between values of $E_{a\tau}$ and $E_{a\sigma}$ obviously indicates that the ionic-hopping mechanism is responsible for the relaxation is same as that for the conductivity [30]. The β values are observed to be almost constant with increasing temperature suggests the insensitivity of temperature.

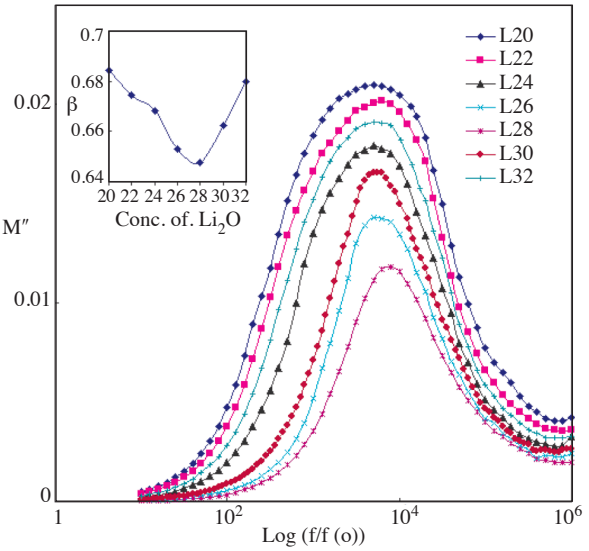

Figure 9. Electric modulus M'' as a function of $\log(f)$ for all the samples of Li_2O-In_2O_3-P_2O_5 glass system measured at 393 K. Inset shows the variation of β with concentration of Li_2O.

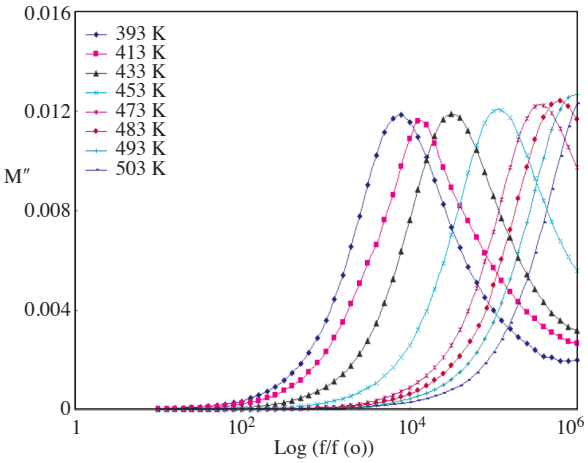

Figure 10. Electric modulus M'' as a function of $\log(f)$ plots for highest conducting sample (L_{28}) at temperatures 393–503 K.

3.4. Scaling analysis

For any data evolution program, scaling analysis is an important feature. To demonstrate that the mechanism of ion transport in the glass system is unaffected by composition and temperature, the Figure 12 is presented. In this figure, the ac conductivity data obtained at various temperatures for L_{28} is scaled

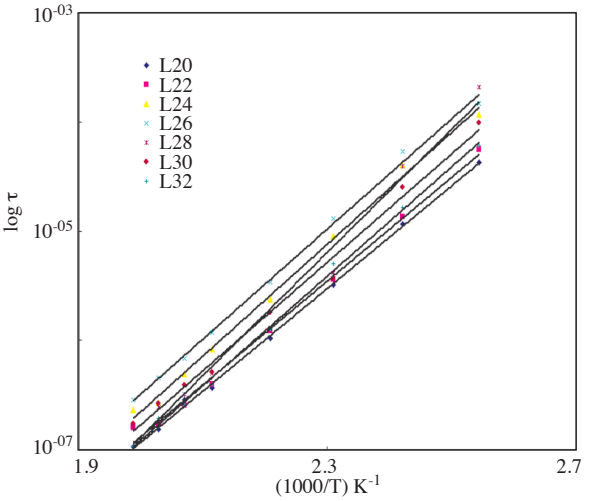

Figure 11. Variation of $\log\ \tau$ as a function of $1000/T$ for all samples of Li_2O-In_2O_3-P_2O_5 glass system.

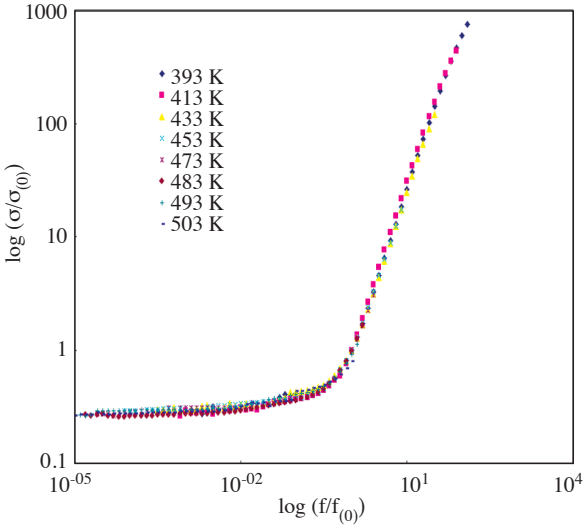

Figure 12. Variation of $\log(\sigma/\ \sigma(0))$ as a function of $\log(f/f_0)$ for highest conducting sample, L_{28}, at temperatures 393–503 K.

with characteristic frequency f_0 and the frequency independent conductivity σ_0 of the frequency axis (x-axis) and ac conductivity axis (y-axis) [31, 32]. In the Figure12, it is observed that all the curves observed at different temperatures fit in to a master curve; this master curve suggests that the present glass samples show evidence of the temperature independent conduction transport mechanism. In the electric modulus spectra, the imaginary electric modulus M'' is scaled with $M''_{\max}$, where $M''_{\max}$ is maximum value of M'' in plots of M'' as a function of $\log(f)$. The electric modulus scaling is expressed as $M''/M''_{\max} = \log(f/f_{\max})$, such scaling electric modulus spectra at different temperatures is shown in Figure 13. The curves in this figure show a high degree of superposition leading to the single master curve at different temperatures. This behavior suggests that temperature independent distribution relaxation time mechanism.

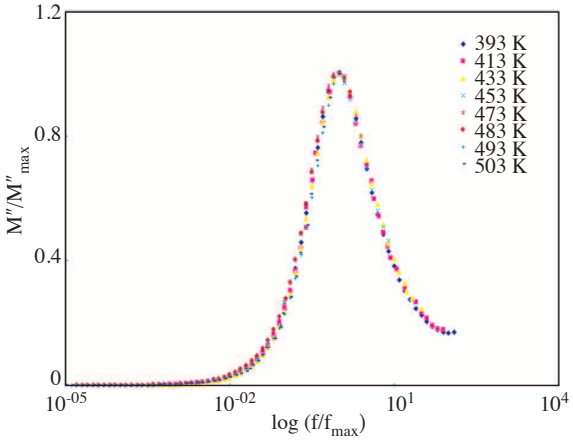

Figure 13. Normalized plots of electric modulus against normalized frequency of the highest conducting sample, L_{28}, at temperatures 393–503 K.

4. Conclusions

The lowest glass forming ability parameter K_{gl} and the glass transition temperature T_g in the differential thermal analysis indicates highest depolymerizability for sample L_{28} among all glass samples investigated. The bulk conductivity of the highest conducting sample, L_{28}, was determined as 1.477×10^{-07} S/cm at 393 K. AC Conductivity data is fitted to a power law equation. The activation energy (0.61 eV) and power exponent s = 0.691 are low for sample L_{28}. The $M''_{\max}$ position of peak frequency shifts towards higher frequency region with the temperature and the stretched exponent factor β is almost constant with increasing temperature. The master curve in normalized plots of both ac conductivity and modulus data suggests that the present glass samples show evidence of the temperature independent conductivity relaxation mechanism.

References

[1] C. A. Angell, *Annu Rev. Phys. Chem.*, **43**, (1992), 693.

[2] K. Otto, *Phys. Chem. Glasses,* **7**, (1986), 35.

[3] K. Minami, F. Mizuno, A. Hayashi, M. Tatsumisago, *Solid State Ionics*, **178**, (2007), 837.

[4] T. J. Minami, *J. Non-Cryst. Solids*, **73**, (1985), 273.

[5] I. Ardelean, C. Andronache, C. Cimpean, P. Pascuta, *Mod. Phys. Lett.* B, **20**, (2006), 105.

[6] K. Yukimitu, E. B. Arau' jo, J. C. S. Moraes, V. C. S. Reynoso, C. L. Carvalho, *J. Phys. D Appl. Phys.,* **35**, (2002), 3229.

[7] L. Bih, M. El Omari, J.-M. Reau, M. Haddad, D. Boudlich, A. Yacoubi, A. Nadiri, *Solid State Ionics,* **132**, (2000), 71.

[8] G. S. Baskaran, G. L. Llower, N. Veeraiah, *J. Alloys Compd.*, **431**, (2007), 303.

[9] M. Srinivasa Reddy, G. Nagaraju, G. Nagarjuna, N. Veeraiah, *J. Alloys Compd.*, **438**, (2007), 41.

[10] I. V. Kityk, J. Ebothe, L. Qingsheng, S. Shaoyong, *J. Fang Nanotechnol.*, **17**, (2006), 1871.

[11] K. Suzuya, C. K. Loong, D. L. Price, B. C. Sales, L. A. Boatner, *J. Non-Cryst. Solids*, **258**, (1999), 48.

[12] N. H. Ray, *Glass. Technol.,* **16**, (1975), 107.

[13] I. V. Kityk, J. Ebothe, Q. Liu, S. Sun, J. Fang, *Nanotechnology,* **17**, (2006), 1871.

[14] J. Koo, B. Soo Bae, H. Kyun Na, *J. Non-Cryst. Solids,* **212**, (1997), 173.

[15] L. F. Maia, A. C. M. Rodrigues, *Solid State Ionics,* **168**, (2004), 87.

[16] P. Kluvanek, R. Klement, M. Karacona, *J. Non-Cryst. Solids,* **353**, (2007), 2004.

[17] A. Mogus-Milankovi, A. S. Santi, M. Karabulut, D. E. Day, *J. Non-Cryst. Solids,* **330**, (2007), 128.

[18] S. Muthupari, S. L. Raghavan, K. J. Rao, *J.Phys. Chem.*, **100**, (1996), 4243

[19] B. Rolling, M. D. Ingram, *J.Non-Cryst.Solids,* **265**, (2002), 113.

[20] S. Khasa, V. P. Seth, A. Agarwal, R. M. Krishna, S. K. Gupta, *Mater. Chem. Phys.*, **72**, (2000), 366.

[21] M. A. L. Nobre, S. Lafendri, *J. Phys.Chem. Solids,* **62**, (2001), 1999.

[22] H. Jain, O. Kanert, in, J. M. Spaeth (Eds.), Proceedings of the XII, International Conference on Defects in insulting materials, vol.1, World Scientific Co., 1993 p. 274.

[23] H. Jain, C. H. Hsieh, *J. Non-Cryst. Solids,* **172**, (1994), 1408.

[24] A. H. Verhoef, H. W. den Hartog, *Solid State Ionics,* **68**, (1994), 305.

[25] S. R. Elliot, A. P. Owens, *Solid State Ionics,* **70**, (1994), 27.

[26] Akira Doi, *J. Mater. Sci.*, **22:3**, (1987), 761.

[27] D. P. Almond, A.R. West, *Solid State Ionics,* **11**, (1983), 57.

[28] Rosario A. Gerhardt, *J. Phys. Chem. Solids,* **55**, (1994), 1491.

[29] C. T. Moynihan, L. P. Boesch, N. L. Laberge, *Phys. Chem. Glasses,* **14**, (1973),122.

[30] B. V. R Chowdari, R. G. Krishnan , S. H. Goh, K. L. Tan, *J. Mater. Sci.*, **23**, (1988), 1248.

[31] A. Ghosh, A. Pan , *Phys. Rev. Lett.,* **84**, (2000), 2188.

[32] T. B. Schroder, J. C. Dyre, *Phys. Rev. Lett.,* **84**, (2000), 310.